# Numerical Simulation of Low Reynolds Number Slip Flow Past a Confined Microsphere

Robert W. Barber and David R. Emerson

*CLRC Daresbury Laboratory, Daresbury, Warrington, Cheshire, WA4 4AD, UK*

**Abstract.** Rapid progress in Micro-Electro-Mechanical Systems (MEMS) technology has led to the development of an increasing number of miniaturised flow devices which involve the manipulation of gases. However, an emerging research issue is the realisation that non-continuum and surface phenomena become increasingly important as devices are reduced in scale. This study investigates the important problem of low Reynolds number rarefied gas flow past a confined microsphere within a circular pipe and focuses on the estimation of the hydrodynamic drag forces on a stationary sphere. Knudsen numbers covering the continuum and slip-flow regimes ($0 \le Kn \le 10^{-1}$) are studied whilst the Reynolds number is varied between $10^{-2} \le Re \le 1$. In addition, blockage effects are investigated by varying the ratio between the diameter of the pipe, $H$, and the diameter of the sphere, $D$. The results indicate that blockage effects are extremely important in the continuum regime and cause an amplification in the hydrodynamic drag. However, blockage phenomena are shown to be less important as the Knudsen number is increased. At the upper limit of the slip-flow regime ($Kn \approx 10^{-1}$), blockage amplification effects are found to be reduced by almost 50% for a pipe-sphere geometry of $H/D = 2$.

## INTRODUCTION

The development of precision fabrication techniques for constructing Micro-Electro-Mechanical-Systems (MEMS) has emerged as one of the most exciting and revolutionary new areas of technology. Miniaturisation of conventional fluidic systems offers a wide range of benefits to the chemical and bio-chemical industries by enabling faster mixing times, improved heat transfer rates, increased chemical yields and faster throughputs for chemical assays [1]. In addition, the small length scales employed in microfluidic systems offer the prospect of developing pressure and chemical sensors having frequency responses in the MHz range.

A variety of advanced microfluidic components are currently being developed including miniaturised heat-exchangers to cool integrated circuits, micro-reactors to generate small quantities of dangerous or expensive chemicals, 'lab-on-a-chip' bio-chemical sensors which perform complex biological assays on sub-nanolitre samples and hand-held gas chromatography systems for the detection of trace concentrations of air-borne pollutants. However, one of the emerging research issues is the realisation that the fluid mechanics in such small scale devices is not the same as that experienced in the macroscopic world.

Early investigations of non-continuum flows in pipes and channels were conducted by researchers in the rarefied gas community who were primarily interested in low-density applications [2,3,4]. However, recent advances in micro-machining technology have enabled flow channels to be constructed with depths of the order of 1 micron leading to a new area of research where rarefied gas behaviour is relevant. For example, experiments conducted by Pfahler *et al.* [5], Harley *et al.* [6] and Arkilic *et al.* [7,8,9] on low Reynolds number gas flows in silicon micro-machined channels have shown that conventional (continuum) analyses are unable to predict the observed flow rates with any degree of accuracy. Consequently, microfluidic systems which are designed simply by scaling-down conventional macro-scale devices may not function as intended.

It has long been established that the continuum assumption in the Navier-Stokes equations is only valid when the mean free path of the molecules is smaller than the characteristic dimension of the flow domain. If this condition is violated, the fluid will no longer be in thermodynamic equilibrium and the linear relationship between the shear stress and rate of shear strain (Newton's law of viscosity) cannot be applied. Velocity profiles, boundary wall shear stresses, mass flow rates and hydrodynamic drag forces will then be influenced by non-continuum effects. Moreover, the conventional no-slip boundary condition imposed at a solid-gas interface begins to break down even

CP663, *Rarefied Gas Dynamics: 23rd International Symposium*, edited by A. D. Ketsdever and E. P. Muntz

before the linear stress-strain relationship becomes invalid (Gad-el-Hak [10]).

For an ideal gas modelled as rigid spheres, the mean free path of the molecules, $\mathcal{L}$, can be related to the temperature, $T$, and pressure, $p$, via

$$\mathcal{L} = \frac{k\,T}{\sqrt{2}\,\pi\,p\,\sigma_c^2} \tag{1}$$

where $k$ is Boltzmann's constant and $\sigma_c$ is the collision diameter of the molecules. The ratio between the mean free path, $\mathcal{L}$, and the characteristic dimension of the flow geometry, $L$, is commonly referred to as the Knudsen number:

$$Kn = \frac{\mathcal{L}}{L}\ . \tag{2}$$

The Knudsen number, $Kn$, determines the degree of rarefaction of the gas and the validity of the continuum hypothesis. Schaaf and Chambre [11] proposed the following classification system based upon the magnitude of the local Knudsen number. For $Kn \le 10^{-2}$, the continuum hypothesis is appropriate and the flow can be analysed using the Navier-Stokes equations with conventional no-slip boundary conditions although Gad-el-Hak [10] has suggested that the breakdown in the continuum assumption is discernible at Knudsen numbers as low as $Kn = 10^{-3}$. When $Kn > 10$, the continuum approach breaks down completely and the regime can then be described as being a *free molecular flow*. Under such conditions, the mean free path of the molecules is far greater than the characteristic length scale and consequently molecules reflected from a solid surface travel, on average, many lengths scales before colliding with other molecules. It is thus valid to neglect the effect of the reflected particles on the incident flow stream, and treat the incident and reflected molecular flows separately. However, for Knudsen numbers between $Kn = 10^{-2}$ and $Kn = 10$, the fluid can neither be considered an absolutely continuous medium nor a free molecular flow. A further sub-classification is therefore necessary to distinguish between the appropriate method of analysis. For $10^{-2} \le Kn \le 10^{-1}$ (commonly referred to as the *slip-flow* regime), the Navier-Stokes equations can still be used provided tangential slip-velocity boundary conditions are implemented along the solid walls of the flow domain. On the other hand, for $10^{-1} \le Kn \le 10$ (*transition flow*), the continuum assumption begins to break down and alternative methods of analysis using the Burnett equations or particle based DSMC (Direct Simulation Monte Carlo) approaches must be employed [12].

In the present work, numerical simulations are used to study the effects of rarefaction on axisymmetric flow past a confined microsphere within a circular pipe. The investigation of rarefied gases by measuring the viscous damping on a rotating sphere dates back to Maxwell and nowadays forms the basis of conventional spinning-rotor vacuum gauges [13,14]. Essentially the rate of damping of an electro-magnetically suspended rotating sphere can be used to measure a number of important properties of a rarefied gas including pressure, viscosity or molecular weight. Similar principles have been envisaged for measuring the flow rates, pressures or viscosities in micro-channels.

## GOVERNING EQUATIONS

The governing hydrodynamic equations for a continuous (infinitely divisible) fluid can be written in tensor notation as follows:

*continuity:*

$$\frac{\partial \rho}{\partial t} + \frac{\partial(\rho\,u_k)}{\partial x_k} = 0 \tag{3}$$

*momentum:*

$$\frac{\partial(\rho\,u_i)}{\partial t} + \frac{\partial(\rho\,u_k\,u_i)}{\partial x_k} = -\frac{\partial p}{\partial x_i} + \frac{\partial \tau_{ik}}{\partial x_k} \tag{4}$$

where $u$ is the velocity, $p$ is the pressure, $\rho$ is the fluid density and $\tau_{ik}$ is the second-order stress tensor. For a Newtonian, isotropic fluid, the stress tensor is given by

$$\tau_{ik} = \mu\left(\frac{\partial u_i}{\partial x_k} + \frac{\partial u_k}{\partial x_i}\right) + \lambda\left(\frac{\partial u_j}{\partial x_j}\right)\delta_{ik} \tag{5}$$

where $\mu$ and $\lambda$ are the first and second coefficients of viscosity and $\delta_{ik}$ is the unit second-order tensor. Implementing Stokes' continuum hypothesis allows the first and second coefficients of viscosity to be related via

$$\lambda + \frac{2}{3}\mu = 0 \tag{6}$$

although the validity of the above equation has occasionally been questioned for fluids other than dilute monatomic gases (Gad-el-Hak [15]).

## Slip-Velocity Boundary Conditions

To account for non-continuum effects in the slip-flow regime ($Kn \leq 10^{-1}$), the Navier-Stokes equations are solved in conjunction with the tangential slip-velocity boundary condition first proposed by Basset [16]:

$$\tau_t = \beta u_t \tag{7}$$

where $u_t$ is the tangential slip-velocity at the wall, $\tau_t$ is the shear stress at the wall and $\beta$ is the slip coefficient. Schaaf and Chambre [11] have shown that the slip coefficient can be related to the mean free path as follows:

$$\beta = \frac{\mu}{\left(\frac{2-\sigma}{\sigma}\right)\mathcal{L}} \tag{8}$$

where $\sigma$ is the tangential momentum accommodation coefficient (TMAC) and $\mathcal{L}$ is the mean free path. The TMAC is introduced to account for gas-surface interactions at the wall. For a perfectly elastic smooth surface, the angles of incidence and reflection of molecules colliding with the wall are identical and therefore the gas cannot exert any stress in the tangential direction. This is referred to as *specular reflection* and results in perfect slip at the boundary ($\sigma \rightarrow 0$). Conversely, in the case of an extremely rough surface, the gas molecules are reflected at totally random angles and lose, on average, their entire tangential momentum: a situation referred to as *diffusive reflection* ($\sigma = 1$).

Experiments indicate that the accommodation coefficient is a function of the molecular weight of the gas, the energy of the incoming molecules, the wall material, the temperature and the condition of the surface. One of the most important parameters affecting the accommodation coefficient is the surface roughness. Porodnov *et al*. [4] conducted experiments on the flow rates of gases through rectangular glass channels with different surface roughness. The experiments for light gases (He, Ne, Ar) indicated a change in the accommodation coefficient from 0.80 to 0.88 when the root-mean square surface roughness was increased from 0.05 μm to 1.5 μm. More recently, Arkilic *et al*. [7,8,9] have measured flow rates in silicon micro-machined channels and extracted accommodation coefficients ranging from 0.8 to 1.0.

Equations (7) and (8) can be combined and rearranged to give

$$u_t = \frac{2-\sigma}{\sigma}\frac{\mathcal{L}}{\mu}\tau_t \ . \tag{9}$$

At this stage it is convenient to recast the mean free path in equation (9) in terms of the non-dimensionalised Knudsen number, *Kn*, which can be defined as the ratio of the mean free path, $\mathcal{L}$, to the diameter of the sphere, *D*:

$$Kn = \frac{\mathcal{L}}{D} \ . \tag{10}$$

Consequently, equation (9) can be recast as

$$u_t = \frac{2-\sigma}{\sigma}\frac{Kn\,D}{\mu}\tau_t \ . \tag{11}$$

The velocity boundary conditions along the walls of the confining pipe can thus be written as

$$u = \frac{2-\sigma}{\sigma}\frac{Kn\,D}{\mu}\tau_t \quad \text{and} \quad v = 0 \qquad \text{on} \qquad r = \frac{H}{2} \tag{12}$$

where *u* and *v* are the velocity components in the longitudinal (*x*) and radial (*r*) directions, respectively, and *H* is the

diameter of the confining pipe. Similarly, the boundary conditions implemented on the surface of the microsphere can be expressed as

$$u_t = \frac{2-\sigma}{\sigma}\frac{Kn\,D}{\mu}\tau_t \quad \text{and} \quad u_n = 0 \qquad \text{on} \qquad x^2 + r^2 = a^2 \tag{13}$$

where $u_t$ is the tangential velocity component, $u_n$ is the normal velocity component and $a$ is the radius of the sphere. The localised velocity vector $(u_t,u_n)$ has to be transformed into the global velocity vector $(u,v)$ using the unit tangential base vector of the surface.

The governing hydrodynamic equations were solved using THOR-2D – a two-dimensional finite-volume Navier-Stokes solver developed by the Computational Engineering Group at CLRC Daresbury Laboratory (Gu and Emerson [17]). Since the flows investigated in the study had relatively low Mach numbers, compressibility effects were ignored and the gas was assumed to be incompressible.

## Inflow/Outflow Boundary Conditions

At the inflow boundary, a fully-developed slip-velocity profile was prescribed parallel to the longitudinal axis of the pipe. The velocity profile for incompressible laminar flow can readily be obtained from the axial-direction momentum equation, as detailed by Barber and Emerson [18]. The inflow boundary conditions can thus be written:

$$u(r) = 2\bar{u}\left(1-\frac{4r^2}{H^2}+4\frac{2-\sigma}{\sigma}\frac{Kn}{H/D}\right)\Bigg/\left(1+8\frac{2-\sigma}{\sigma}\frac{Kn}{H/D}\right) \quad \text{and} \quad v(r)=0 \qquad \text{at} \qquad x=-l \;,\; 0\le r\le\frac{H}{2} \tag{14}$$

where $\bar{u}$ is the mean velocity in the pipe and $l$ is the longitudinal distance between the inflow boundary and the centre of the sphere. As an aside, in the limit of $Kn \to 0$ (i.e. continuum flow conditions), equation (14) reverts to the familiar no-slip (NS) velocity profile given by Hagen-Poiseuille pipe theory:

$$u_{\mathrm{NS}}(r) = 2\bar{u}\left(1-\frac{4r^2}{H^2}\right). \tag{15}$$

At the outlet, the axial gradients of the velocity components were assumed to be zero, i.e.

$$\frac{\partial u}{\partial x}=0 \quad \text{and} \quad \frac{\partial v}{\partial x}=0 \qquad \text{at} \qquad x=l \;,\; 0\le r\le\frac{H}{2} \;. \tag{16}$$

## RESULTS AND DISCUSSION

The numerical model was used to assess the drag experienced by a confined microsphere exposed to low Reynolds number rarefied gas flows. For compatibility with previous simulations [19], the Reynolds number, *Re*, was defined using the mean velocity in the pipe, $\bar{u}$ , and the radius of the sphere, *a*, as the velocity and length scales:

$$Re = \frac{\rho\,\bar{u}\,a}{\mu} \tag{17}$$

whilst the Knudsen number was defined using the diameter of the sphere as the characteristic length scale. Following Liu *et al*. [19], the simulations considered extremely low Reynolds numbers corresponding to the creeping flow conditions originally analysed by Stokes. The Knudsen number was varied from $Kn = 0$ (continuum flow) to $Kn = 10^{-1}$ (a frequently adopted upper bound for the slip-flow regime). In the absence of additional information, the tangential momentum accommodation coefficient, $\sigma$, was assumed to have a value of unity.

Blockage effects were studied by varying the ratio between the diameter of the confining pipe, *H*, and the diameter of the sphere, *D*. The simulations involved a range of blockage ratios from $H/D = 2$ up to $H/D = 40$.

## Continuum Flow Regime

The numerical model was validated in the continuum regime by comparing the computed drag on the sphere against the numerical results presented by Liu *et al*. [19] and the analytical solution developed by Haberman and

Sayre [20]. Unconfined creeping flow past a sphere was first analysed by Stokes who demonstrated that in the absence of inertial forces, the total drag due to the flow of an unbounded incompressible Newtonian fluid could be written as

$$\text{Total drag} = 6\pi\mu U\, a \tag{18}$$

where $U$ denotes the uniform velocity distribution infinitely far from the sphere. Non-dimensionalising the drag by the dynamic pressure and the cross-sectional area of the sphere allows the drag coefficient, $C_D$, to be written as

$$C_D = \frac{\text{Total drag}}{\frac{1}{2}\rho U^2 \pi a^2} = \frac{6\pi\mu U\, a}{\frac{1}{2}\rho U^2 \pi a^2} = \frac{12\mu}{\rho U\, a} = \frac{12}{Re'} \tag{19}$$

where the Reynolds number, $Re'$, is defined using the velocity of the *unbounded* fluid. The drag coefficient for an unconfined sphere can thus be rearranged to give:

$$\frac{C_D\, Re'}{12} = 1 \ . \tag{20}$$

In a similar manner, the drag coefficient for a *confined* sphere can be determined using an analogous equation to that shown in (19), except that the dynamic pressure is defined in terms of the *mean* velocity in the pipe, $\bar{u}$ :

$$C_D = \frac{\text{Total drag}}{\frac{1}{2}\rho \bar{u}^2 \pi a^2} \ . \tag{21}$$

The drag coefficient can then be normalised using the procedure adopted by Liu *et al*. [19] to give

$$\frac{C_D\, Re}{12} = \mathcal{F}(H/D) \tag{22}$$

where $\mathcal{F}(H/D)$ denotes a function of blockage ratio. The above equation has obvious similarities with the unconfined solution developed in equation (20), with the exception that the product of the drag coefficient and the Reynolds number no longer collapses to a single value but instead depends upon the blockage ratio. Moreover, it is important to note that the Reynolds number must be defined in terms of the average velocity in the pipe rather than the unbounded velocity used in Stokes' unconfined solution.

Figure 1 presents the normalised drag predictions for a range of blockage ratios from $H/D = 2$ to $H/D = 40$ for a Reynolds number, $Re = 0.125$ (as adopted by Liu *et al*. [19]). The results show that the sphere experiences significant blockage effects for $H/D < 10$ with a very large increase in the drag coefficient being observed for $H/D < 5$. The computed drag results presented by Liu *et al*. [19] for $H/D < 5$ are superimposed on Figure 1 for comparison purposes. In the limit of $H/D \to \infty$, the normalised drag should converge asymptotically to the value predicted by Stokes' unconfined solution. As the blockage ratio is increased, the average velocity striking the sphere and contributing to the drag will approach the maximum (centreline) velocity in the pipe, $2\bar{u}$. The normalised drag coefficient will therefore tend to a value of 2 for large blockage ratios, i.e.

$$\frac{C_D Re}{12} \to 2 \qquad \text{as} \qquad H/D \to \infty \ . \tag{23}$$

Figure 1 clearly shows that the computed normalised drag coefficients tend to the theoretical asymptote presented in equation (23).

A further validation of the numerical scheme was achieved using the analytical drag formula presented by Haberman and Sayre [20] who investigated axisymmetric flow past a confined sphere using an algebraic stream function approach. Normalising the equation presented by Haberman and Sayre yields

$$\frac{C_D Re}{12} = 2\left(1 - \frac{2}{3}\frac{D^2}{H^2} - 0.20217\frac{D^5}{H^5}\right) \Bigg/ \left(1 - 2.1050\frac{D}{H} + 2.0865\frac{D^3}{H^3} - 1.7068\frac{D^5}{H^5} + 0.72603\frac{D^6}{H^6}\right) . \tag{24}$$

The excellent agreement between the numerical predictions and the analytical solution over the entire range of blockage ratios indicates that the computational scheme provides an accurate representation of the flow past a confined sphere and demonstrates the accuracy of the numerical drag computations.

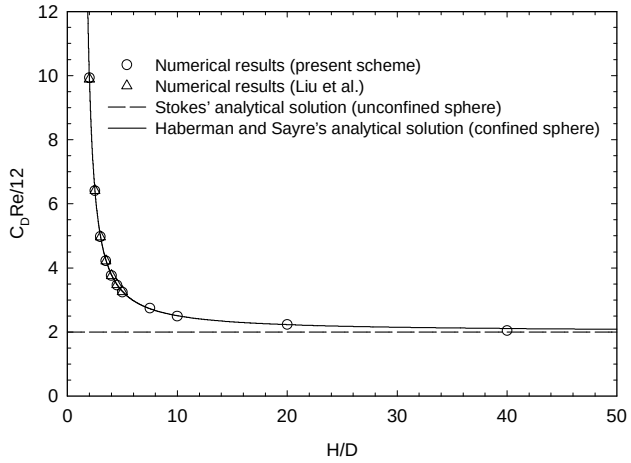


**FIGURE 1.** Variation of normalised total drag coefficient on a confined sphere as a function of blockage ratio in the continuum flow regime (*Kn*=0).

## Slip-Flow Regime

The second part of the study investigated the drag experienced by the sphere in the slip-flow regime. Simulations were conducted using Reynolds numbers in the range, $10^{-2} \leq Re \leq 1$ whilst the Knudsen number was varied up to $Kn = 10^{-1}$ (the upper limit of the slip-flow regime). A fully-developed slip-velocity profile (equation 14) was prescribed at the inflow boundary to simulate an infinitely long pipe upstream of the computational domain and the fluid was again assumed to be incompressible on account of the low Mach numbers found in most microfluidic devices. Additional numerical simulations accounting for compressibility showed very little difference in the predicted drag on the sphere, justifying the low Mach number simplification.

In an incompressible Newtonian fluid, it can be shown that the normal stress component must vanish along any rigid no-slip impermeable boundary (Richardson [21]). In contrast, the tangential slip-velocity boundary condition in rarefied gas flows generates a non-zero normal stress component which produces an important additional drag force on the sphere.

Normalised drag results for the least confined blockage ratio ($H/D$ = 40) provide a useful validation of the hydrodynamic code since the results should approach the asymptotic limit of low Reynolds number slip flow past an unconfined sphere. Barber and Emerson [22] have previously described an extension of Stokes' analytical solution for creeping flow past a sphere which accounts for non-continuum effects. The analysis follows the methodology originally proposed by Basset [16] and provides expressions for the total drag and the individual drag components experienced by an unconfined sphere in the slip-flow regime. The total drag can be shown to be given by

$$\text{Total drag} = 6\pi\mu U a \left(1 + 4\frac{2-\sigma}{\sigma} Kn\right) \Big/ \left(1 + 6\frac{2-\sigma}{\sigma} Kn\right) \tag{25}$$

whilst the individual drag components are given by

$$\text{Skin-friction drag} = 4\pi\mu U a \Big/ \left(1 + 6\frac{2-\sigma}{\sigma} Kn\right), \tag{26}$$

$$\text{Normal stress drag} = 4\pi\mu U a \left(4\frac{2-\sigma}{\sigma} Kn\right) \Big/ \left(1 + 6\frac{2-\sigma}{\sigma} Kn\right) \tag{27}$$

and

$$\text{Pressure drag} = 2\pi\mu U a \left(1 + 4\frac{2-\sigma}{\sigma} Kn\right) \Big/ \left(1 + 6\frac{2-\sigma}{\sigma} Kn\right). \tag{28}$$

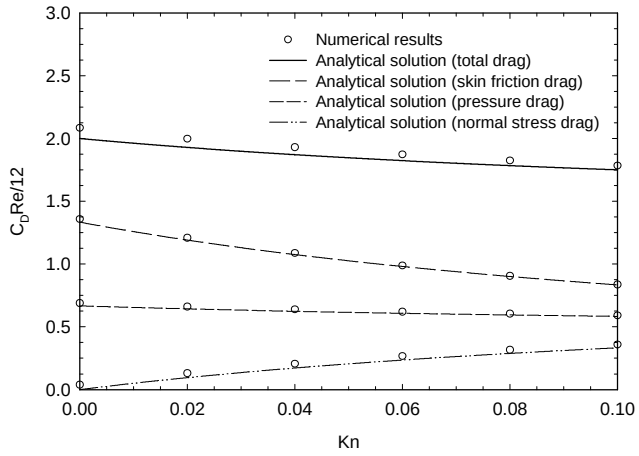


**FIGURE 2.** Variation of normalised drag coefficients on a confined sphere in the slip-flow regime as a function of Knudsen number ($H/D$ = 40).

Figure 2 illustrates the variation in normalised drag components on the sphere as a function of Knudsen number for a blockage ratio of $H/D$ = 40. It should be noted than in normalising the analytical drag equations (25-28), the unconfined drag components have been multiplied by a factor of 2 to account for the parabolic velocity profile in the pipe. Small discrepancies can be seen in the normal stress drag predictions which in turn affect the total drag. This can be confirmed by noting that the numerical model fails to predict a zero normal stress drag component in the continuum flow regime ($Kn$ = 0). Previous numerical studies by Beskok and Karniadakis [23] on rarefied gas flows past circular cylinders have confirmed the difficulty in obtaining accurate estimates of the normal stress distribution. Nevertheless, the general agreement between the predictions and the unconfined analytical solution provides an important validation test in the slip-flow regime.

Finally, Figure 3 illustrates the variation in normalised total drag coefficient with Knudsen number for three separate blockage ratios. In the slip-flow regime, the total drag on the sphere decreases as the Knudsen number is increased. More importantly, the results indicate that the drag amplification effect caused by the blockage ratio becomes less significant as rarefaction starts to influence the flow. At the upper limit of the slip-flow regime ($Kn = 10^{-1}$), blockage amplification effects are reduced by almost 50% for a pipe-sphere geometry of $H/D$ = 2. It should be noted that the tangential momentum accommodation coefficient, $\sigma$, is assumed to have a value of unity in the present simulations. However, a sub-unity accommodation coefficient would further reduce the blockage amplification effect.

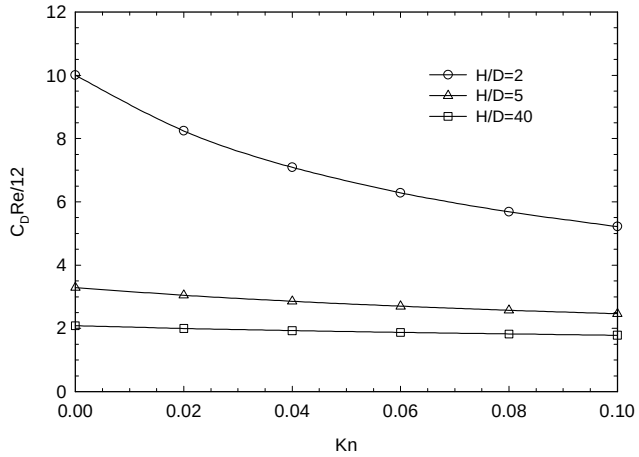


**FIGURE 3.** Variation of normalised total drag coefficient on a confined sphere in the slip-flow regime as a function of Knudsen number.

## CONCLUSIONS

Low Reynolds number rarefied flow past a confined microsphere has been investigated using a specially adapted two-dimensional finite-volume Navier-Stokes solver. The hydrodynamic model is applicable to the continuum and slip-flow regimes, and is valid for Knudsen numbers in the range $0 \leq Kn \leq 10^{-1}$. At low Reynolds numbers in the continuum regime, the results show that the product of the drag coefficient and the Reynolds number collapses to a single value dependent upon the blockage ratio, $H/D$. The results also indicate that blockage effects are extremely important for continuum flows, with very large increases in the drag being observed for $H/D < 5$. In the slip-flow regime, the total drag on the sphere decreases as the Knudsen number is increased. More importantly, the results suggest that the drag amplification effect caused by blockage ratio becomes less significant as rarefaction starts to influence the flow. This may have important consequences for the design of microfluidic components which operate over a wide range of Knudsen numbers.

## REFERENCES


1. Wegeng, R.S., Call, C.J., and Drost, M.K., "Chemical System Miniaturisation", Paper no. PNNL-SA-27317, Spring National Meeting of A.I.Chem.E., New Orleans, 1996.
2. Ebert, W.A., and Sparrow, E.M., *Trans. ASME, J. Basic Eng.* **87**, 1018-1024 (1965).
3. Sreekanth, A.K, "Slip Flow Through Long Circular Tubes" in *Rarefied Gas Dynamics* **6**, Academic Press, 1968, pp. 667-680.
4. Porodnov, B.T., Suetin, P.E., Borisov, S.F., and Akinshin, V.D., *J. Fluid Mech.* **64**, 417-437 (1974).
5. Pfahler, J., Harley, J., Bau, H.H., and Zemel, J.N., *Micromechanical Sensors, Actuators and Systems*, DSC-Vol. 32, 49-60 (1991).
6. Harley, J.C., Huang, Y., Bau, H.H., and Zemel, J.N., *J. Fluid Mech*. **284**, 257-274 (1995).
7. Arkilic, E.B., Breuer, K.S., and Schmidt, M.A., *Application of Microfabrication to Fluid Mechanics*, FED-Vol. 197, *ASME*, 57-66 (1994).
8. Arkilic, E.B., Schmidt, M.A., and Breuer, K.S., *J. Micro-Electro-Mechanical Systems* **6**, 167-178 (1997).
9. Arkilic, E.B., Schmidt, M.A., and Breuer, K.S., "TMAC Measurement in Silicon Micromachined Channels" in *Rarefied Gas Dynamics* **20**, Beijing University Press (1997).
10. Gad-el-Hak, M., *Trans. ASME, J. Fluids Engineering* **121**, 5-33 (1999).
11. Schaaf, S.A., and Chambre, P.L., *Flow of Rarefied Gases*, Princeton University Press, 1961.
12. Bird, G.A., *Molecular Gas Dynamics and the Direct Simulation of Gas Flows*, Clarendon Press, 1994.
13. Reich, G., *J. Vacuum Science and Technology* **20**, 1148-1152 (1982).
14. Fremerey, J.K, *J. Vacuum Science and Technology* **A 3**, 1715-1720 (1985).
15. Gad-el-Hak, M., *Trans. ASME, J. Fluids Engineering* **117**, 3-5 (1995).
16. Basset, A.B., *A Treatise on Hydrodynamics*, Cambridge University Press, 1888.
17. Gu, X.J., and Emerson, D.R., *THOR-2D: A Two-Dimensional Computational Fluid Dynamics Code*, Technical Report, Computational Science and Engineering Department, CLRC Daresbury Laboratory, 2000.
18. Barber, R.W., and Emerson, D.R., *A Numerical Study of Low Reynolds Number Slip Flow in the Hydrodynamic Development Region of Circular and Parallel Plate Ducts*, Technical Report DL-TR-00-002, Computational Science and Engineering Department, CLRC Daresbury Laboratory, December 2000.
19. Liu, H-C.F., Beskok, A., Gatsonis, N., and Karniadakis, G.E., *Micro-Electro-Mechanical Systems (MEMS)*, DSC-Vol. 66, *ASME*, 445-452 (1998).
20. Haberman, W.L., and Sayre, R.M., *Motion of Rigid and Fluid Spheres in Stationary and Moving Liquids Inside Cylindrical Tubes*, David Taylor Model Basin Report No. 1143, U.S. Navy Dept., Washington D.C., 1958.
21. Richardson, S.M., *Fluid Mechanics*, Hemisphere Publishing Corp., 1989.
22. Barber, R.W., and Emerson, D.R., *Analytical Solution of Low Reynolds Number Slip Flow Past a Sphere*, Technical Report DL-TR-00-001, Computational Science and Engineering Department, CLRC Daresbury Laboratory, December 2000.
23. Beskok, A., and Karniadakis, G.E., *J. Thermophysics and Heat Transfer* **8**, 647-655 (1994).